
Estimation of the Body Segment Inertial Parameters for the Rigid Body Biomechanical Models Used in Motion Analysis

Raphaël Dumas and Janis Wojtusich

Abstract

Body segment inertial parameters (BSIPs) of the human body are key parameters in biomechanics to study the dynamics of human motion. BSIPs can be obtained in different ways including direct measurements on cadavers or photogrammetry and medical imaging on living humans, but they are more generally estimated by regression equations (based on those measurements).

This chapter overviews three widely used regression equations reported by Winter (2009), de Leva (1996a), and Dumas et al. (2007a). These regression equations are presented for the head with neck, thorax, abdomen, pelvis, and right upper arm, forearm, hand, thigh, shank, and foot segments.

The segment endpoints and segment reference frames defined at the time of the BSIPs assessment and regression computation are reviewed so that the reader can consider how they match with the construction of the rigid body biomechanical models they would like to use for motion analysis. The segment definitions and regression equations that remain undefined or unavailable are indicated, and some assumptions are proposed to amend them, where found applicable. The computation of the segment mass, position of center of mass, moments, and products of inertia from these regression equations are fully detailed, including the modification of the designation of the segment axes and the transformation from right to left segments.

R. Dumas (✉)

LBMCMR_T9406, Univ Lyon, Université Claude Bernard Lyon 1, IFSTTAR, Lyon, France
e-mail: raphael.dumas@ifsttar.fr

J. Wojtusich

Department of Computer Science, Simulation, Systems Optimization and Robotics Group, TU Darmstadt, Darmstadt, Germany
e-mail: wojtusch@sim.tu-darmstadt.de

Keywords

Segment mass • Center of mass • Moments of inertia • Regression equations • Segment length • Segment endpoints • Joint center • Segment reference frame

Contents

Introduction	2
State of the Art	3
Computation of the BSIPs from the Regression Equations	4
Segment Definition and Regression Equations	6
Future Directions	6
References	29

Introduction

Body segment inertial parameters (BSIPs) are required in biomechanics for the computation of intersegmental moments, angular momentum, mechanical work, and for the study of the whole body dynamic stability (see “► [3D Kinetics of Human Motion](#),” “► [Induced Acceleration and Induced Power Analyses of Human Motion](#),” “► [Optimal Control Modeling of Human Movement](#),” and “► [Physics-based Models for Human Gait Analysis](#)”). BSIPs refer to the segment mass, the position of the segment center of mass with respect to a segment reference frame, and the segment moments and products of inertia with respect to a segment point (typically the segment center of mass or a segment endpoint) and with respect to a segment reference frame (see “► [Three-dimensional Reconstruction of the Human Skeleton in Motion](#)”).

BSIPs of the human body can be obtained in different ways. The history and the description of the techniques used to assess BSIPs can be found in Pearsall and Reid [1994](#), Reid and Jensen [1990](#), and Drillis et al. [1964](#). BSIPs can be directly measured on cadavers (Dempster [1955](#); Clauser et al. [1969](#); Chandler et al. [1975](#)) and indirectly measured on living subjects, typically through photogrammetry (Ackland et al. [1988](#); Jensen [1978](#); McConville et al. [1980](#); Young et al. [1983](#)) or medical imaging (Bauer et al. [2007](#); Dumas et al. [2005](#); Durkin et al. [2002](#); Mungiole and Martin [1990](#); Pearsall et al. [1996](#); Zatsiorsky et al. [1990](#); Cheng et al. [2000](#)). Based on these measurements, estimations of the BSIPs from regression equations are more classically used. Obviously, these regression equations are limited by the number and the nature of the subjects on which they have been established. In other words, regression equations for BSIPs are better established for older Caucasian non-pathological males than for females, children, and, as a matter of fact, for pathological subjects. Nevertheless, regression equations are widely used because of their expediency.

Furthermore, when studying the dynamics of human motion with a 3D rigid body biomechanical model, another difficulty is to match the segment definition used for the BSIP assessment with the model construction. Indeed, BSIPs have been obtained with their own rationale for segment endpoints and segment reference frames, generally constrained by experimental and technical limitations. Conversely, rigid

body biomechanical models (see “► [Rigid Body Models of the Musculoskeletal System](#)” in this book) and especially “conventional gait models” widely used in clinical motion analysis (Davis et al. 1991; Kadaba et al. 1990) (see “► [Conventional Gait Model – Success and Limitations](#)” in this book), are based on a chosen marker set and calibration protocol that aims at approximating the joint centers and axes. In this context, several adjustment procedures of existing regression equations have been proposed (de Leva 1996a; Dumas et al. 2007a; Hinrichs 1990) for a better correspondence between segment definition and model construction. Still, no specific adjustment for “conventional gait models” has been proposed, and it is commonly assumed that the segment definition used for the BSIP assessment and the model construction are consistent. Therefore, classically, the segment center of mass is expected to align with the axis linking the joint centers, and this axis plus two orthogonal axes are expected to be principal axes of inertia.

This chapter overviews three widely used sets of regression equations for BSIPs, allowing for a 16-segment rigid body biomechanical model. The segment definitions (i.e., segment endpoints and segment axes or planes) used for the BSIP assessment, regression computation, and adjustment are reviewed so that the reader can consider how they match with the construction of the “conventional gait models” or any rigid body biomechanical models they would like to use.

The segment definitions and regression equations that remain undefined or unavailable are specified, and some assumptions are proposed to amend them, where found applicable. Note that the planes of segmentation used for the BSIP assessment can be also an issue (leading to some differences between the regression equations, especially for the trunk segments), but, conversely to the segment endpoints, axes, and planes, this does not directly interfere with the construction of the biomechanical models used in motion analysis and this is not reviewed in this chapter.

State of the Art

Three widely used regression equations for BSIP are the regression equations of Winter (2009) derived from the data of Dempster (1955), the regression equations of de Leva (1996a) adjusted from the data of Zatsiorsky et al. (1990), and the regression equations of Dumas et al. (2007a, b) adjusted from the data of McConville et al. (1980) and Young et al. (1983).

Dempster (1955) directly measured the BSIPs of eight male cadavers (mean age 68.5 years old, mean weight 61.1 kg, mean stature 1.69 m) using equilibrium and pendulum methods. Zatsiorsky et al. (1990) indirectly measured the BSIPs by frontal gamma-ray scanner on 100 males (mean age 23.8 years old, mean weight 73.0 kg, mean stature 1.74 m) and 15 females (mean age 19.0 years old, mean weight 61.9 kg, mean stature 1.73 m). They obtained the surface density of the body from subjects lying supine. The foot segment was scanned in a lateral view separately from the rest of the body. The whole human body was modeled as rectangular cuboids of 2 cm width and length and of different heights estimated from anthropometric measurements. The masses and the distances from the geometrical centers of the cuboids to

reference anatomical landmarks were known from the surface density. The centers of the mass of the cuboids were assumed at their geometrical centers and the principal axes of inertia of the cuboids were assumed aligned with the axes of symmetry of the cuboids. Then, the BSIPs of the segments were computed by summing up the BSIPs of the cuboids (i.e., using weighted barycenter and parallel axis theorem). McConville et al. (1980) and Young et al. (1983) indirectly measured the BSIPs by photogrammetry on 31 males (mean age 27.5 years old, mean weight 77.3 kg, mean stature 1.77 m) and 46 females (mean age 31.2 years old, mean weight 63.9 kg, mean stature 1.61 m), respectively. The BSIPs are defined relative to skin anatomical landmarks assuming a homogenous density of 1 g/cm^3 .

Based on these datasets and according to the aforementioned adjustments, linear regression equations have been proposed (de Leva 1996a; Dumas et al. 2007a; Winter 2009). The segment mass is computed as a percentage of the body mass. The position of the center of mass is computed as a percentage of the segment length, defined as the distance between the segment endpoints. The radii of gyration (i.e., the square roots of the moments of inertia divided by the segment mass) are computed as percentages of the segment length. In these regression equations, the number of segments is 16: the head with neck, thorax, abdomen, pelvis, right and left upper arms, forearms and hands, and thighs, shanks, and feet.

In the literature, other segmentations and other regression equations (i.e., nonlinear (Zatsiorsky et al. 1990), involving anthropometric measurements such as segment circumferences (Yeadon and Morlock 1989; Zatsiorsky et al. 1990)) exist but appear hardly used, probably because they do not fit well with the motion analysis protocols (i.e., they involve not only skin markers but also calipers and tape measures).

Computation of the BSIPs from the Regression Equations

As previously mentioned, the segment mass, m_s , of segment $s = 1, \dots, 16$ is estimated as:

$$m_s = p_s M \quad (1)$$

where p_s is the percentage of the body mass M .

The position of the center of mass with respect to the segment reference frame is estimated as:

$$\mathbf{r}_s = L_s \begin{pmatrix} c_s^X \\ c_s^Y \\ c_s^Z \end{pmatrix} \quad (2)$$

where c_s^X, c_s^Y, c_s^Z are coordinates of the center of mass expressed as percentages of the segment length L_s .

The inertia matrix (moments and products of inertia in and out the diagonal, respectively) with respect to the center of mass and the segment reference frame is estimated as:

$$\mathbf{I}_s = m_s(L_s)^2 \begin{bmatrix} (r_s^{XX})^2 & (r_s^{XY})^2 & (r_s^{XZ})^2 \\ & (r_s^{YY})^2 & (r_s^{YZ})^2 \\ \text{sym.} & & (r_s^{ZZ})^2 \end{bmatrix} \quad (3)$$

where $r_s^{XX}, r_s^{YY}, r_s^{ZZ}$ are radii of gyration (i.e., the square roots of the moments of inertia divided by the segment mass) expressed as percentages of the segment length L_s . The products of inertia are expressed in the same way (i is indicated in case of negative products of inertia).

The designation of the segment axes can be different from one rigid body biomechanical model to another. The regression equations in the following tables will be labeled with respect to the anterior-posterior, superior-inferior, and medial-lateral axes. These labels are intended for a subject in anatomic posture (standing upright with arms at the sides, palms facing forward, and feet parallel). Note that in the “conventional gait models,” **I** axis is anterior, **J** axis is lateral (to the left), and **K** axis is superior (Davis III et al. 1991; Kadaba et al. 1990). However, according to the standardization of the *International Society of Biomechanics* (ISB), **X** axis is anterior, **Y** axis is superior, and **Z** axis is lateral (to the right) (Wu et al. 2002, 2005). The sign convention used in the following tables complies with this standardization of the ISB (**X**, **Y**, and **Z** axes). Nevertheless, the position of the center of mass and the inertia matrix with respect to the **I**, **J**, and **K** axes can be easily computed using a permutation matrix **P**:

$$\mathbf{r}_s = \underbrace{\begin{bmatrix} 1 & 0 & 0 \\ 0 & 0 & 1 \\ 0 & -1 & 0 \end{bmatrix}}_{\mathbf{P}} L_s \begin{pmatrix} c_s^X \\ c_s^Y \\ c_s^Z \end{pmatrix} \quad (4)$$

and

$$\mathbf{I}_s = m_s(L_s)^2 [\mathbf{P}] \begin{bmatrix} (r_s^{XX})^2 & (r_s^{XY})^2 & (r_s^{XZ})^2 \\ & (r_s^{YY})^2 & (r_s^{YZ})^2 \\ \text{sym.} & & (r_s^{ZZ})^2 \end{bmatrix} [\mathbf{P}]^T. \quad (5)$$

In the same way, the regression equations in the following tables are for the right upper and lower limb segments. The position of the center of mass and the inertia matrix for the left segments can be computed (in the **X**, **Y**, and **Z** axes) using a symmetry matrix **S** (in place of **P**) in Eqs. 4 and 5:

$$\mathbf{S} = \begin{bmatrix} 1 & 0 & 0 \\ 0 & 1 & 0 \\ 0 & 0 & -1 \end{bmatrix}. \quad (6)$$

The inertia matrix (moments and products of inertia) in Eq. 3 is given with respect to the center of mass and the segment reference frame. The inertia matrix with

respect to the origin of the segment reference frame can be computed with the parallel axis theorem:

$$\mathbf{I}_s^* = \mathbf{I}_s + m_s \left(\left((\mathbf{r}_s)^T \mathbf{r}_s \right) \mathbf{E}_{3 \times 3} - \mathbf{r}_s (\mathbf{r}_s)^T \right) \quad (7)$$

where $\mathbf{E}_{3 \times 3}$ is the identity matrix.

Segment Definition and Regression Equations

For the regression equations of Winter (2009), the BSIPs for the segments of the trunk are revised based on the original data of Dempster (1955) and the additional estimations of Plagenhoef (1971): the center of mass of the abdomen and pelvis segments was estimated by equilibrium methods applied to a cardboard-lead cutout modeling the anthropometry and mass distribution of the trunk as reported by Dempster (1955).

Note that, in the original data of Dempster (1955), only an abdominopelvic segment is reported. Its mass is 26.4% of body mass and its segment density is 1.01 g/cm^3 . The position of its center of mass about the superior-inferior axis is -59.9% of segment length (i.e., thoracic joint center to midpoint between hip joint centers). The abdomen and pelvis segments are presented in the following tables for consistency among the different regression equations. Nevertheless, this abdominopelvic segment may be preferred if this segmentation matches with the rigid body biomechanical model used for motion analysis. Moreover, the abdomen and pelvis segments were also available in the regression equations reported by Winter (2009), but the position of the center of mass of these segments, as well as the thorax segment, was given in percentage of the longitudinal distance between midpoints between glenohumeral and hip joint centers (i.e., 30.4% of total height (Plagenhoef 1971)).

As for the regression equations based on the data of McConville et al. (1980) and Young et al. (1983), the regression equations provided in the following tables include updates for the thorax and abdomen segments (Dumas et al. 2015) and a revision made for this chapter (i.e., some typos and inconsistency in the regression equations for the joint centers previously used in the adjustment procedure were corrected).

The segment endpoints and segment axes are presented in Fig. 1 with the related skin landmarks and joint centers estimated by different regression equations. The regression equations for the BSIPs of the different segments are given in (Tables 1–10).

Future Directions

As previously mentioned in the introduction, regression equations (specifically regression equations based on body mass and segment lengths) are widely used because of their expediency but remain limited and sometimes difficult to harmonize with the rigid body biomechanical models used for motion analysis.

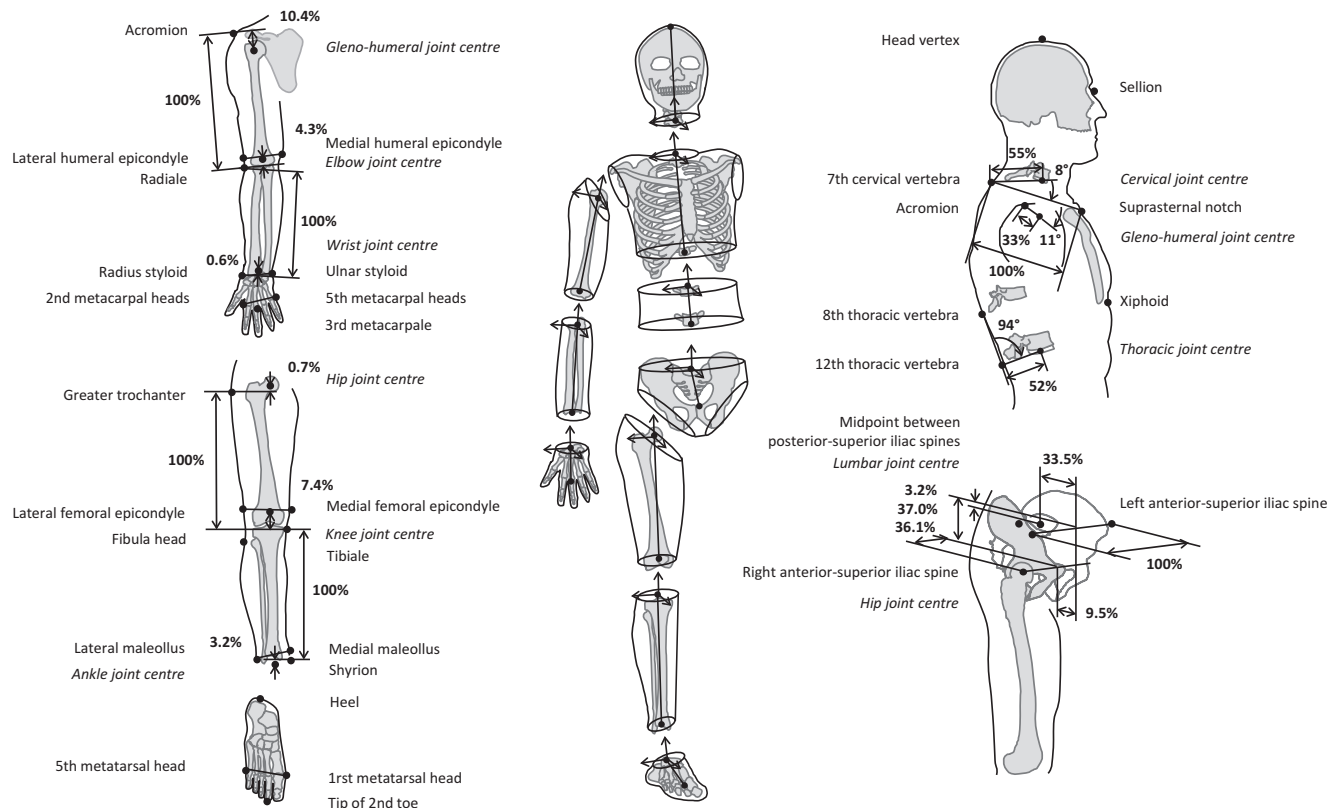


Fig. 1 Skin landmarks, joint centers estimated by regression equations, and body segments

Table 1 Head with neck

The head with neck		(Dempster 1955; Winter 2009)	(de Leva 1996a; Zatsiorsky et al. 1990)	(Dumas et al. 2007b; McConville et al. 1980; Young et al. 1983)
Segment endpoints		Head vertex skin landmark ^a Cervical joint center obtained by dissection (center of C7-T1 disc)	Skin landmark on head vertex projected on superior-inferior axis Skin landmark on 7th cervical vertebra projected on superior-inferior axis	Skin landmark on the head vertex Cervical joint center estimated by the regression equations (Dumas et al. 2007a) Female: cervical joint center on a direction forming an angle of 14° in the sagittal plane with the vector from 7th cervical vertebra to suprasternal notch skin landmarks and at 53% of the thorax width (i.e., distance between 7th cervical vertebra and suprasternal notch skin landmarks) from 7th cervical vertebra skin landmark Male: angle of 8° and percentage of 55%
Segment reference frame		Superior-inferior axis from cervical joint center to head vertex skin landmark Sagittal plane set as plane of oscillation of the pendulum method Origin at head vertex skin landmark ^a	Superior-inferior axis: <i>N/A</i> Frontal plane parallel to the gamma-ray scanner acquisition plane Origin at head vertex skin landmark projected on superior-inferior axis	Superior-inferior axis from cervical joint center to head vertex skin landmark Sagittal plane containing cervical joint center and skin landmarks on the head vertex and sellion Origin at cervical joint center
Segment length (mm)		<i>N/A</i>	Female: 243.7 and male: 242.9	Female: 243 and male: 278
Segment density (g/cm ³)		1.11	<i>N/A</i>	<i>Assumed to be 1</i>
Segment mass (% of total body mass)		Female: <i>N/A</i> and male: 8.10	Female: 6.68 and male: 6.94	Female: 6.7 and male: 6.7

(continued)

Table 1 (continued)

The head with neck		(Dempster 1955; Winter 2009)	(de Leva 1996a; Zatsiorsky et al. 1990)	(Dumas et al. 2007b; McConville et al. 1980; Young et al. 1983)
Position of center of mass (% of the segment length)	Anterior-posterior axis (X)	<i>Assumed negligible</i>	<i>N/A</i>	Female: 0.8 and male: 2.0
	Superior-inferior axis (Y)	Female: <i>N/A</i> and male: -43.3^a	Female: -48.41 and male: -50.02	Female: 55.9 and male: 53.4
	Medial-lateral axis (Z)	<i>Assumed negligible</i>	<i>Assumed negligible</i>	Female: -0.1 and male: 0.1
Moment of inertia (radius of gyration in % of the segment length)	Anterior-posterior axis (X)	<i>Assumed equal to medial-lateral axis</i>	Female: 29.5 and male: 31.5	Female: 30 and male: 28
	Superior-inferior axis (Y)	<i>N/A</i>	Female: 26.1 and male: 26.1	Female: 24 and male: 21
	Medial-lateral axis (Z)	Female: <i>N/A</i> and male: 28.1^a	Female: 27.1 and male: 30.3	Female: 31 and male: 30
Product of inertia	Sagittal plane (X,Y)	<i>Assumed negligible</i>	<i>Assumed negligible</i>	Female: 5(i) and male: 7(i)
	Transverse plane (X, Z)	<i>Assumed negligible</i>	<i>Assumed negligible</i>	Female: 1 and male: 2(i)
	Frontal plane (Y,Z)	<i>Assumed negligible</i>	<i>Assumed negligible</i>	Female: 0 and male: 3

^aValue of Winter (2009) replaced by original value of Dempster (1955), radius of gyration worked out with a rule of 3

Table 2 Thorax

The thorax		(Dempster 1955; Winter 2009)	(de Leva 1996a; Zatsiorsky et al. 1990)	(Dumas et al. 2015; McConville et al. 1980; Young et al. 1983)
Segment endpoints		Cervical joint center (see head with neck segment) Thoracic joint center obtained by dissection (center of T12-L1 disc)	Skin landmark on the seventh cervical vertebra projected on superior-inferior axis Skin landmark on xiphoid projected on superior-inferior axis	Cervical joint center (see head with neck segment) Thoracic joint center estimated by the regression equations (Dumas et al. 2015) Female: thoracic joint center on a direction forming an angle of 92° in the sagittal plane with the vector from 12th to 8th thoracic vertebra skin landmarks and at 50% of thorax width (see head with neck segment) from 12th thoracic vertebra skin landmark Male : angle of 94° and percentage of 52%
Segment reference frame		Superior-inferior axis from thoracic to cervical joint center Sagittal plane set as plane of oscillation of the pendulum method Origin at cervical joint center	Superior-inferior axis: <i>N/A</i> Frontal plane parallel to the gamma-ray scanner acquisition plane Origin at 7th cervical vertebra skin landmark projected on superior-inferior axis	Superior-inferior axis from thoracic to cervical joint center Sagittal plane containing skin landmarks on 7th cervical and 8th thoracic vertebra and suprasternal notch Origin at cervical joint center
Segment length (mm)		<i>N/A</i>	Female: 228.0 and male: 242.1	Female: 322 and male: 334
Segment density (g/cm ³)		0.92	<i>N/A</i>	<i>Assumed to be 1</i>
Segment mass (% of total body mass)		Female: <i>N/A</i> and male: 21.60	Female: 15.45 and male: 15.96	Female: 26.3 and male: 30.4
Position of center of mass (% of the segment length)	Anterior-posterior axis (X)	<i>Assumed negligible</i>	<i>N/A</i>	Female: 1.5 and male: 0.0
	Superior-inferior axis (Y)	Female: <i>N/A</i> and male: -62.7°	Female: -50.50 and male: -50.66	Female: -54.2 and male: -55.5
	Medial-lateral axis (Z)	<i>Assumed negligible</i>	<i>Assumed negligible</i>	Female: 0.1 and male: -0.4


(continued)

Table 2 (continued)

The thorax		(Dempster 1955; Winter 2009)	(de Leva 1996a; Zatsiorsky et al. 1990)	(Dumas et al. 2015; McConville et al. 1980; Young et al. 1983)
Moment of inertia (radius of gyration in % of the segment length)	Anterior-posterior axis (X)	<i>N/A</i>	Female: 31.4 and male: 32.0	Female: 38 and male: 42
	Superior-inferior axis (Y)	<i>N/A</i>	Female: 44.9 and male: 46.5	Female: 32 and male: 33
	Medial-lateral axis (Z)	<i>N/A</i>	Female: 46.6 and male: 50.5	Female: 34 and male: 36
Product of inertia	Sagittal plane (X, Y)	<i>N/A</i>	<i>N/A</i>	Female: 12(i) and male: 11(i)
	Transverse plane (X,Z)	<i>Assumed negligible</i>	<i>Assumed negligible</i>	Female: 3(i) and male: 1
	Frontal plane (Y, Z)	<i>Assumed negligible</i>	<i>Assumed negligible</i>	Female: 1 and male: 3

^aValue of Winter (2009) replaced by original value of Dempster (1955)

Table 3 Abdomen

The abdomen		(Dempster 1955; Plagenhoef 1971; Winter 2009)	(de Leva 1996a; Zatsiorsky et al. 1990)	(Dumas et al. 2015; McConville et al. 1980; Young et al. 1983)
Segment endpoints		Thoracic joint center (see thorax segment) Inferior endpoint: <i>N/A</i>	Skin landmark on xiphoid projected on superior-inferior axis Skin landmark on omphalion projected on superior-inferior axis	Thoracic joint center (see thorax segment) Lumbar joint center estimated by the regression equations (Dumas et al. 2007a) Female: in the pelvis reference frame (see pelvis segment) with origin translated at midpoint between anterior-superior iliac spine skin landmarks, lumbar joint center at -34.0% , 4.9% and 0% of pelvis width (see pelvis segment) about the anterior-posterior, superior-inferior, and medial-lateral axes, respectively Male: percentages of -33.5% , -3.2% , and 0.0% , respectively
Segment reference frame		Superior-inferior axis: <i>N/A</i> Sagittal plane of the cardboard-lead cutouts modeling the anthropometry and mass distribution of the trunk Origin at thoracic joint center ^a	Superior-inferior axis: <i>N/A</i> Frontal plane parallel to the gamma-ray scanner acquisition plane Origin at xiphoid skin landmark projected on superior-inferior axis	Superior-inferior axis from thoracic to lumbar joint center Sagittal plane  <i>N/A</i> (no axial rotation at lumbar joint center assumed) Origin at thoracic joint center
Segment length (mm)		<i>N/A</i>	Female: 205.3 and male: 215.5	Female: 125 and male: 151
Segment density (g/cm ³)		<i>N/A</i>	<i>N/A</i>	<i>Assumed to be 1</i>

(continued)

Table 3 (continued)

The abdomen		(Dempster 1955; Plagenhoef 1971; Winter 2009)	(de Leva 1996a; Zatsiorsky et al. 1990)	(Dumas et al. 2015; McConville et al. 1980; Young et al. 1983)
Segment mass (% of total body mass)		Female: <i>N/A</i> and male: 13.90	Female: 14.65 and male: 16.33	Female: 4.1 and male: 2.9
Position of center of mass (% of the segment length)	Anterior-posterior axis (X)	<i>N/A</i>	<i>N/A</i>	Female: 21.9 and male: 17.6
	Superior-inferior axis (Y)	Female: <i>N/A</i> and male: -34.6^a	Female: -45.12 and male: -45.02	Female: -41.0 and male: -36.1
	Medial-lateral axis (Z)	<i>Assumed negligible</i>	<i>Assumed negligible</i>	Female: 0.3 and male: -3.3
Moment of inertia (radius of gyration in % of the segment length)	Anterior-posterior axis (X)	<i>N/A</i>	Female: 35.4 and male: 38.3	Female: 65 and male: 54
	Superior-inferior axis (Y)	<i>N/A</i>	Female: 41.5 and male: 46.8	Female: 78 and male: 66
	Medial-lateral axis (Z)	<i>N/A</i>	Female: 43.3 and male: 48.2	Female: 52 and male: 40
Product of inertia	Sagittal plane (X,Y)	<i>N/A</i>	<i>N/A</i>	Female: 25 and male: 11
	Transverse plane (X,Z)	<i>Assumed negligible</i>	<i>Assumed negligible</i>	Female: 3(i) and male: 6(i)
	Frontal plane (Y,Z)	<i>Assumed negligible</i>	<i>Assumed negligible</i>	Female: 5(i) and male: 5(i)

^aAdapted from Plagenhoef (1971), position of center of mass expressed as percentage of the length of the abdominopelvic segment (thoracic joint center to the midpoint between the hip joint centers)

Table 4 Pelvis

The pelvis		(Dempster 1955; Plagenhoef 1971; Winter 2009)	(de Leva 1996a; Zatsiorsky et al. 1990)	(Dumas et al. 2007a; McConville et al. 1980; Young et al. 1983)
Segment endpoints		Superior endpoint: <i>N/A</i> Midpoint between hip joint centers obtained by dissection (acetabulum center)	Skin landmark on omphalion projected on superior-inferior axis Midpoint between hip joint centers estimated by the regression equations (de Leva 1996b) Female: <i>N/A</i> Male: on superior-inferior axis, hip joint center at 0.7% of thigh length (i.e., longitudinal distance between tibial and greater trochanter skin landmarks) from the greater trochanter skin landmark (percentages on anterior-posterior and media-lateral axes: <i>N/A</i>)	Lumbar joint center (see abdomen segment) Midpoint between hip joint centers estimated by the regression equations (Dumas et al. 2007a) Female: in the pelvis reference frame (see below) with origin translated at midpoint between anterior-superior iliac spine skin landmarks, right/left hip joint center at -13.9% , -33.6% , and $\pm 37.2\%$ of pelvis width (i.e., distance between left and right anterior-superior iliac spine skin landmarks) about the anterior-posterior, superior-inferior, and medial-lateral axes, respectively Male: percentages of -9.5% , -37.0% , and $\pm 36.1\%$, respectively
Segment reference frame		Superior-inferior axis: <i>N/A</i> Sagittal plane of the cardboard-lead cutouts modeling the anthropometry and mass distribution of the trunk Origin at midpoint between hip joint centers	Superior-inferior axis: <i>N/A</i> Frontal plane parallel to the gamma-ray scanner acquisition plane Origin at omphalion skin landmark projected on superior-inferior axis	Medial-lateral axis from left to right anterior superior iliac spine skin landmarks Transverse plane containing skin landmarks on left and right anterior-superior iliac spines and midpoint between posterior-superior iliac spines Origin at lumbar joint center
Segment length (mm)		<i>N/A</i>	Female: 181.5 and male: 145.7	Female: 103 and male: 93
Segment density (g/cm ³)		<i>N/A</i>	<i>N/A</i>	<i>Assumed to be 1</i>

(continued)

Table 4 (continued)

The pelvis		(Dempster 1955; Plagenhoef 1971; Winter 2009)	(de Leva 1996a; Zatsiorsky et al. 1990)	(Dumas et al. 2007a; McConville et al. 1980; Young et al. 1983)
Segment mass (% of total body mass)		Female: <i>N/A</i> and male: 14.20	Female: 12.47 and male: 11.17	Female: 14.7 and male: 14.2
Position of center of mass (% of the segment length)	Anterior-posterior axis (X)	<i>N/A</i>	<i>N/A</i>	Female: -7.2 and male: -0.2
	Superior-inferior axis (Y)	Female: <i>N/A</i> and male: -15.6 ^a	Female: -49.20 and male: -61.15	Female: -22.8 and male: -28.2
	Medial-lateral axis (Z)	<i>Assumed negligible</i>	<i>Assumed negligible</i>	Female: 0.2 and male: -0.6
Moment of inertia (radius of gyration in % of the segment length)	Anterior-posterior axis (X)	<i>N/A</i>	Female: 40.2 and male: 55.1	Female: 95 and male: 102
	Superior-inferior axis (Y)	<i>N/A</i>	Female: 44.4 and male: 58.7	Female: 105 and male: 106
	Medial-lateral axis (Z)	<i>N/A</i>	Female: 43.3 and male: 61.5	Female: 82 and male: 96
Product of inertia	Sagittal plane (X,Y)	<i>N/A</i>	<i>N/A</i>	Female: 35(i) and male: 25(i)
	Transverse plane (X,Z)	<i>Assumed negligible</i>	<i>Assumed negligible</i>	Female: 3(i) and male: 12(i)
	Frontal plane (Y,Z)	<i>Assumed negligible</i>	<i>Assumed negligible</i>	Female: 2(i) and male: 8(i)

^aAdapted from Plagenhoef (1971), position of center of mass expressed as percentage of the length of the abdominopelvic segment (thoracic joint center to the midpoint between the hip joint centers)

Table 5 Upper arm

The upper arm		(Dempster 1955; Plagenhoef 1971; Winter 2009)	(de Leva 1996a; Zatsiorsky et al. 1990)	(Dumas et al. 2007a; McConville et al. 1980; Young et al. 1983)
Segment endpoints		Glenohumeral joint center obtained by dissection (center of curvature of humeral head) Elbow joint center obtained by dissection (axis of humeral trochlea at narrowest cross section of ulnar articulation)	Glenohumeral and elbow joint centers estimated by the regression equations (de Leva 1996b) Female: <i>N/A</i> Male: on superior-inferior axis, glenohumeral joint center at 10.4% of upper arm length (i.e., longitudinal distance between acromion and radial skin landmarks) from acromion skin landmark and elbow joint center at 4.3% of upper arm length from radial skin landmark (percentages on anterior-posterior and media-lateral axes: <i>N/A</i>)	Glenohumeral joint center estimated by the regression equations (Dumas et al. 2007a) Elbow joint center estimated at midpoint between lateral and medial humeral epicondyle skin landmarks Female : glenohumeral joint center on a direction forming an angle of 5° in the sagittal plane with the vector from 7th cervical vertebra to suprasternal notch skin landmarks and at 36% of thorax width (see head with neck and thorax segments) from the acromion skin landmark Male: angle of 11° and percentage of 33%
Segment reference frame		Superior-inferior axis from elbow to glenohumeral joint center Sagittal plane set as plane of oscillation of the pendulum method Origin at glenohumeral joint center	Superior-inferior axis from elbow to glenohumeral joint center Frontal plane parallel to the gamma-ray scanner acquisition plane Origin at glenohumeral joint center	Superior-inferior axis from elbow to glenohumeral joint center Frontal plane containing glenohumeral joint center and skin landmarks on lateral and medial humeral epicondyles Origin at glenohumeral joint center
Segment length (mm)		Female: <i>N/A</i> and male: 286 ^a	Female: 275.1 and male: 281.7	Female: 251 and male: 277
Segment density (g/cm ³)		1.07	<i>N/A</i>	<i>Assumed to be 1</i>

(continued)

Table 5 (continued)

The upper arm		(Dempster 1955; Plagenhoef 1971; Winter 2009)	(de Leva 1996a; Zatsiorsky et al. 1990)	(Dumas et al. 2007a; McConville et al. 1980; Young et al. 1983)
Segment mass (% of total body mass)		Female: <i>N/A</i> and male: 2.80	Female: 2.55 and male: 2.71	Female: 2.3 and male: 2.4
Position of center of mass (% of the segment length)	Anterior-posterior axis (X)	<i>Assumed negligible</i>	<i>Assumed negligible</i>	Female: -5.5 and male: 1.8
	Superior-inferior axis (Y)	Female: <i>N/A</i> and male: -43.6	Female: -57.54 and male: -57.72	Female: -50.0 and male: -48.2
	Medial-lateral axis (Z)	<i>Assumed negligible</i>	<i>Assumed negligible</i>	Female: -3.3 and male: -3.1
Moment of inertia (radius of gyration in % of the segment length)	Anterior-posterior axis (X)	<i>Assumed equal to medial-lateral axis</i>	Female: 26.0 and male: 26.9	Female: 30 and male: 29
	Superior-inferior axis (Y)	<i>N/A</i>	Female: 14.8 and male: 15.8	Female: 15 and male: 13
	Medial-lateral axis (Z)	Female: <i>N/A</i> and male: 32.2	Female: 27.8 and male: 28.5	Female: 30 and male: 30
Product of inertia	Sagittal plane (X, Y)	<i>Assumed negligible</i>	<i>Assumed negligible</i>	Female: 3(i) and male: 5
	Transverse plane (X,Z)	<i>Assumed negligible</i>	<i>Assumed negligible</i>	Female: 5 and male: 3
	Frontal plane (Y,Z)	<i>Assumed negligible</i>	<i>Assumed negligible</i>	Female: 3 and male: 13(i)

^aValue of Plagenhoef (1971), 16.9% of total height

Table 6 Forearm

The forearm		(Dempster 1955; Plagenhoef 1971; Winter 2009)	(de Leva 1996a; Zatsiorsky et al. 1990)	(Dumas et al. 2007a; McConville et al. 1980; Young et al. 1983)
Segment endpoints		Elbow joint center (see upper arm segment) Wrist joint center obtained by dissection (center of curvature of proximal end of capitate bone)	Elbow joint center (see upper arm segment) Wrist joint center estimated by the regression equations (de Leva 1996b) Female: <i>N/A</i> Male: on superior-inferior axis, wrist joint center at 0.6% of forearm length (i.e., longitudinal distance between radial and radius styloid skin landmarks) from radius styloid skin landmark (percentages on anterior-posterior and media-lateral axes: <i>N/A</i>)	Elbow joint center (see upper arm segment) Wrist joint center estimated at midpoint between radial and ulna styloid skin landmarks
Segment reference frame		Superior-inferior axis from wrist to elbow joint center Sagittal plane set as plane of oscillation of the pendulum method Origin at elbow joint center	Superior-inferior axis from wrist to elbow joint center Frontal plane parallel to the gamma-ray scanner acquisition plane Origin at elbow joint center	Superior-inferior axis from wrist to elbow joint center Frontal plane containing elbow joint center and skin landmarks on radial and ulna styloids Origin at elbow joint center
Segment length (mm)		Female: <i>N/A</i> and male: 269 ^a	Female: 264.3 and male: 268.9	Female: 247 and male: 283
Segment density (g/cm ³)		1.13	<i>N/A</i>	<i>Assumed to be 1</i>
Segment mass (% of total body mass)		Female: <i>N/A</i> and male: 1.60	Female: 1.38 and male: 1.62	Female: 1.4 and male: 1.7

(continued)

Table 6 (continued)

The forearm		(Dempster 1955; Plagenhoef 1971; Winter 2009)	(de Leva 1996a; Zatsiorsky et al. 1990)	(Dumas et al. 2007a; McConville et al. 1980; Young et al. 1983)
Position of center of mass (% of the segment length)	Anterior-posterior axis (X)	<i>Assumed negligible</i>	<i>Assumed negligible</i>	Female: 2.1 and male: -1.3
	Superior-inferior axis (Y)	Female: <i>N/A</i> and male: -43.0	Female: -45.59 and male: -45.74	Female: -41.1 and male: -41.7
	Medial-lateral axis (Z)	<i>Assumed negligible</i>	<i>Assumed negligible</i>	Female: 1.9 and male: 1.1
Moment of inertia (radius of gyration in % of the segment length)	Anterior-posterior axis (X)	<i>Assumed equal to medial-lateral axis</i>	Female: 25.7 and male: 26.5	Female: 27 and male: 28
	Superior-inferior axis (Y)	<i>N/A</i>	Female: 9.4 and male: 12.1	Female: 14 and male: 11
	Medial-lateral axis (Z)	Female: <i>N/A</i> and male: 30.3	Female: 26.1 and male: 27.6	Female: 25 and male: 28
Product of inertia	Sagittal plane (X,Y)	<i>Assumed negligible</i>	<i>Assumed negligible</i>	Female: 10 and male: 8
	Transverse plane (X,Z)	<i>Assumed negligible</i>	<i>Assumed negligible</i>	Female: 3 and male: 1(i)
	Frontal plane (Y,Z)	<i>Assumed negligible</i>	<i>Assumed negligible</i>	Female: 13(i) and male: 2

^aValue of Plagenhoef (1971), 15.9% of total height

Table 7 Hand

The hand		(Dempster 1955; Winter 2009)	(de Leva 1996a; Zatsiorsky et al. 1990)	(Dumas et al. 2007a; McConville et al. 1980; Young et al. 1983)
Segment endpoints		Wrist joint center (see forearm segment) Interphalangeal knuckle of 3rd finger skin landmark	Wrist joint center (see forearm segment) 3rd metacarpal skin landmark projected on superior-inferior axis	Wrist joint center (see forearm segment) Midpoint between 2nd and 5th metacarpal head skin landmarks
Segment reference frame		Superior-inferior axis: <i>N/A</i> Sagittal plane set as plane of oscillation of the pendulum method Origin at wrist joint center	Superior-inferior axis: <i>N/A</i> Frontal plane parallel to the gamma-ray scanner acquisition plane Origin at wrist joint center	Superior-inferior axis from midpoint between 2nd and 5th metacarpal head skin landmarks to wrist joint center Frontal plane containing wrist joint center and skin landmarks on 2nd and 5th metacarpal heads Origin at wrist joint center
Segment length (mm)		<i>N/A</i>	Female: 78.0 and male: 86.2	Female: 71 and male: 80
Segment density (g/cm ³)		1.17	<i>N/A</i>	<i>Assumed to be 1</i>
Segment mass (% of total body mass)		Female: <i>N/A</i> and male: 0.60	Female: 0.56 and male: 0.61	Female: 0.5 and male: 0.6
Position of center of mass (% of the segment length)	Anterior-posterior axis (X)	<i>N/A</i>	<i>N/A</i>	Female: 7.7 and male: 8.2
	Superior-inferior axis (Y)	Female: <i>N/A</i> and male: -50.6	Female: -74.74 and male: -79.00	Female: -76.8 and male: -83.9
	Medial-lateral axis (Z)	<i>Assumed negligible</i>	<i>Assumed negligible</i>	Female: 4.8 and male: 7.5

(continued)

Table 7 (continued)

The hand		(Dempster 1955; Winter 2009)	(de Leva 1996a; Zatsiorsky et al. 1990)	(Dumas et al. 2007a; McConville et al. 1980; Young et al. 1983)
Moment of inertia (radius of gyration in % of the segment length)	Anterior-posterior axis (X)	<i>N/A</i>	Female: 45.4 and male: 51.3	Female: 64 and male: 61
	Superior-inferior axis (Y)	<i>N/A</i>	Female: 33.5 and male: 40.1	Female: 43 and male: 38
	Medial-lateral axis (Z)	Female: <i>N/A</i> and male: 29.7	Female: 53.1 and male: 62.8	Female: 59 and male: 56
Product of inertia	Sagittal plane (X,Y)	<i>N/A</i>	<i>Assumed negligible</i>	Female: 29 and male: 22
	Transverse plane (X,Z)	<i>N/A</i>	<i>Assumed negligible</i>	Female: 23 and male: 15
	Frontal plane (Y,Z)	<i>N/A</i>	<i>Assumed negligible</i>	Female: 28(i) and male: 20(i)

Table 8 Thigh

The thigh		(Dempster 1955; Plagenhoef 1971; Winter 2009)	(de Leva 1996a; Zatsiorsky et al. 1990)	(Dumas et al. 2007a; McConville et al. 1980; Young et al. 1983)
Segment endpoints		Hip joint center obtained by dissection (center of curvature of femoral head) Knee joint center obtained by dissection (middle of a line through the center of curvature of the posterior aspect of femoral condyles)	Hip joint center (see pelvis segment) Knee joint center estimated by the regression equations (de Leva 1996b) Female: <i>N/A</i> Male: on superior-inferior axis, knee joint center at 7.4% of thigh length (i.e., longitudinal distance between greater trochanter and tibial skin landmarks) from tibial skin landmark (percentages on anterior-posterior and media-lateral axes: <i>N/A</i>)	Hip joint center (see pelvis segment) Knee joint center estimated at midpoint between midpoint between lateral and medial femoral epicondyle skin landmarks
Segment reference frame		Superior-inferior axis from knee to hip joint center Sagittal plane set as plane of oscillation of the pendulum method Origin at hip joint center	Superior-inferior axis from knee to hip joint center Frontal plane parallel to the gamma-ray scanner acquisition plane Origin at hip joint center	Superior-inferior axis from knee to hip joint center Frontal plane containing hip joint center and skin landmarks on lateral and medial femoral epicondyles
Segment length (mm)		Female: <i>N/A</i> and male: 395 ^a	Female: 368.5 and male: 422.2	Female: 379 and male: 432
Segment density (g/cm ³)		1.05	<i>N/A</i>	<i>Assumed to be 1</i>
Segment mass (% of total body mass)		Female: <i>N/A</i> and male: 10.00	Female: 14.78 and male: 14.16	Female: 14.6 and male: 12.3

(continued)

Table 8 (continued)

The thigh		(Dempster 1955; Plagenhoef 1971; Winter 2009)	(de Leva 1996a; Zatsiorsky et al. 1990)	(Dumas et al. 2007a; McConville et al. 1980; Young et al. 1983)
Position of center of mass (% of the segment length)	Anterior-posterior axis (X)	<i>Assumed negligible</i>	<i>Assumed negligible</i>	Female: -7.7 and male: -4.1
	Superior-inferior axis (Y)	Female: <i>N/A</i> and male: -43.3	Female: -36.12 and male: -40.95	Female: -37.7 and male: -42.9
	Medial-lateral axis (Z)	<i>Assumed negligible</i>	<i>Assumed negligible</i>	Female: 0.8 and male: 3.3
Moment of inertia (radius of gyration in % of the segment length)	Anterior-posterior axis (X)	<i>Assumed equal to medial-lateral axis</i>	Female: 36.4 and male: 32.9	Female: 31 and male: 29
	Superior-inferior axis (Y)	<i>N/A</i>	Female: 16.2 and male: 14.9	Female: 19 and male: 15
	Medial-lateral axis (Z)	Female: <i>N/A</i> and male: 32.3	Female: 36.9 and male: 32.9	Female: 32 and male: 30
Product of inertia	Sagittal plane (X,Y)	<i>Assumed negligible</i>	<i>Assumed negligible</i>	Female: 7(i) and male: 7
	Transverse plane (X,Z)	<i>Assumed negligible</i>	<i>Assumed negligible</i>	Female: 2 and male: 2(i)
	Frontal plane (Y,Z)	<i>Assumed negligible</i>	<i>Assumed negligible</i>	Female: 7(i) and male: 7(i)

^aValue of Plagenhoef (1971), 23.4% of total height

Table 9 Shank

The shank		(Dempster 1955; Plagenhoef 1971; Winter 2009)	(de Leva 1996a; Zatsiorsky et al. 1990)	(Dumas et al. 2007a; McConville et al. 1980; Young et al. 1983)
Segment endpoints		Knee joint center (see thigh segment) Ankle joint center obtained by dissection (center of the area of the cut body of the talus)	Knee joint center (see thigh segment) Ankle joint center estimated by the regression equations (de Leva 1996b) Male: on superior-inferior axis, ankle joint center at 3.2% of shank length (i.e., longitudinal distance between tibial and sphyrion skin landmarks) from sphyrion skin landmark (percentages on anterior-posterior and media-lateral axes: <i>N/A</i>)	Knee joint center (see thigh segment) Ankle joint center estimated at midpoint between lateral and medial malleolus skin landmarks
Segment reference frame		Superior-inferior axis from ankle to knee joint center Sagittal plane set as plane of oscillation of the pendulum method Origin at knee joint center	Superior-inferior axis from ankle to knee joint center Frontal plane parallel to the gamma-ray scanner acquisition plane Origin at knee joint center	Superior-inferior axis from ankle to knee joint center Frontal plane containing knee and ankle joint centers and the fibula head skin landmark Origin at knee joint center
Segment length (mm)		Female: <i>N/A</i> and male: 428 ^a	Female: 438.6 and male: 440.3	Female: 388 and male: 433
Segment density (g/cm ³)		1.09	<i>N/A</i>	<i>Assumed to be 1</i>
Segment mass (% of total body mass)		Female: <i>N/A</i> and male: 4.65	Female: 4.81 and male: 4.33	Female: 4.5 and male: 4.8

(continued)

Table 9 (continued)

The shank		(Dempster 1955; Plagenhoef 1971; Winter 2009)	(de Leva 1996a; Zatsiorsky et al. 1990)	(Dumas et al. 2007a; McConville et al. 1980; Young et al. 1983)
Position of center of mass (% of the segment length)	Anterior-posterior axis (X)	<i>Assumed negligible</i>	<i>Assumed negligible</i>	Female: -4.9 and male: -4.8
	Superior-inferior axis (Y)	Female: <i>N/A</i> and male: -43.3	Female: -43.52 and male: -43.95	Female: -40.4 and male: -41.0
	Medial-lateral axis (Z)	<i>Assumed negligible</i>	<i>Assumed negligible</i>	Female: 3.1 and male: 0.7
Moment of inertia (radius of gyration in % of the segment length)	Anterior-posterior axis (X)	<i>Assumed equal to medial-lateral axis</i>	Female: 26.3 and male: 24.6	Female: 28 and male: 28
	Superior-inferior axis (Y)	<i>N/A</i>	Female: 9.2 and male: 10.2	Female: 10 and male: 10
	Medial-lateral axis (Z)	Female: <i>N/A</i> and male: 30.2	Female: 26.7 and male: 25.1	Female: 28 and male: 28
Product of inertia	Sagittal plane (X,Y)	<i>Assumed negligible</i>	<i>Assumed negligible</i>	Female: 2 and male: 4(i)
	Transverse plane (X,Z)	<i>Assumed negligible</i>	<i>Assumed negligible</i>	Female: 1 and male: 2(i)
	Frontal plane (Y,Z)	<i>Assumed negligible</i>	<i>Assumed negligible</i>	Female: 6 and male: 4

^aValue of Plagenhoef (1971), 25.3% of total height

Table 10 Foot

The foot		(Dempster 1955; Winter 2009)	(de Leva 1996a; Zatsiorsky et al. 1990)	(Dumas et al. 2007a; McConville et al. 1980; Young et al. 1983)
Segment endpoints		Heel skin landmarks ^a Tip of 2nd toe skin landmarks ^a	Heel skin landmark Tip of longest toe skin landmark	Ankle joint center (see shank segment) Midpoint between 1st and 5th metatarsal head skin landmarks
Segment reference frame		Anterior-posterior axis from heel to tip of 2nd toe skin landmarks Sagittal plane set as plane of oscillation of the pendulum method Origin at heel skin landmark ^a	Anterior-posterior axis from heel to tip of longest toe skin landmarks Frontal plane parallel to the gamma-ray scanner acquisition plane Origin at heel skin landmark	Anterior-posterior axis from heel to midpoint between 1st and 5th metatarsal head skin landmarks Transverse plane containing skin landmarks on heel and 1st and 5th metatarsal heads
Segment length (mm)		<i>N/A</i>	Female: 228.3 and male: 258.1	Female: 117 and male: 139
Segment density (g/cm ³)		1.09	<i>N/A</i>	<i>Assumed to be 1</i>
Segment mass (% of total body mass)		Female: <i>N/A</i> and male: 1.45	Female: 1.29 and male: 1.37	Female: 1.0 and male: 1.2
Position of center of mass (% of the segment length)	Anterior-posterior axis (X)	Female: <i>N/A</i> and male: 42.9 ^a	Female: 40.14 and Male: 44.15	Female: 38.2 and male: 50.2
	Superior-inferior axis (Y)	<i>Assumed negligible</i>	<i>Assumed negligible</i>	Female: −30.9 and male: −19.9
	Medial-lateral axis (Z)	<i>Assumed negligible</i>	<i>Assumed negligible</i>	Female: 5.5 and male: 3.4

(continued)

Table 10 (continued)

The foot		(Dempster 1955; Winter 2009)	(de Leva 1996a; Zatsiorsky et al. 1990)	(Dumas et al. 2007a; McConville et al. 1980; Young et al. 1983)
Moment of inertia (radius of gyration in % of the segment length)	Anterior-posterior axis (X)	<i>N/A</i>	Female: 13.9 and male: 12.4	Female: 24 and male: 22
	Superior-inferior axis (Y)	<i>Assumed equal to medial-lateral axis</i>	Female: 27.9 and male: 24.5	Female: 50 and male: 49
	Medial-lateral axis (Z)	Female: <i>N/A</i> and male: 40.7 ^a	Female: 29.9 and male: 25.7	Female: 50 and male: 48
Product of inertia	Sagittal plane (X,Y)	<i>N/A</i>	<i>N/A</i>	Female: 15(i) and male: 17
	Transverse plane (X,Z)	<i>N/A</i>	<i>N/A</i>	Female: 9 and male: 11(i)
	Frontal plane (Y,Z)	<i>Assumed negligible</i>	<i>Assumed negligible</i>	Female: 5(i) and male: 0

^aValue of Winter (2009) replaced by original value of Dempster (1955), radius of gyration worked out with a rule of 3

The adaptation of the previously developed adjustment procedures to elderly subjects has been recently proposed (Ho Hoang and Mombaur 2015) and may be extended to other specific populations.

There is an increasing interest in using subject-specific BSIPs of the lower limb indirectly measured by medical imaging (Bauer et al. 2007; Dao et al. 2012; Ganley and Powers 2004; Sreenivasa et al. 2016; Taddei et al. 2012; Valente et al. 2014) for gait analysis, especially in case of pathologic subjects (see “► [Cross-platform Comparison of Imaging Technologies for Measuring Musculoskeletal Motion](#)”). Here again, the issue of matching segment definition used for the BSIP assessment with the biomechanical model used for motion analysis exists. The segment definition and model construction are generally assumed consistent or anatomical landmarks are virtually palpated on the MRI or CT scan reconstructions (Dao et al. 2012; Sreenivasa et al. 2016; Valente et al. 2014). Occasionally, skin markers are placed on the subject before CT scan and gait analysis, both performed consecutively (Taddei et al. 2012). Nevertheless, the main purpose of these cumbersome personalization methods was generally focussed on bone and muscle geometry.

The introduction of skin markers used for motion analysis within the procedure of the BSIPs assessment was more widely adopted with photogrammetry (Davidson et al. 2008; Pillet et al. 2010; Verriest 2012). This means that calibrated photographs are taken during a static posture (just before or after motion analysis) allowing to build a 3D volume model of the subject, straightforwardly registered with the rigid body biomechanical model.

Moreover, without additional calibrated photographs and not performed during a static posture but a dynamic movement, the BSIPs can be estimated by identification methods (Ayusawa et al. 2014; Jovic et al. 2016; Vaughan et al. 1982). In this case, a rigid body biomechanical model and the equations of motion are directly used to compute the BSIPs that minimize the errors between model-derived and measured ground reaction forces and moments. However, as for the functional calibration of the joint centers and axes, these methods may require dedicated movements. With that respect, a method that simultaneously identifies BSIPs, joint centers, and segment lengths has been recently proposed (Bonnet et al. 2017). This method, based on extended Kalman filters, minimizes the errors between model-derived and measured ground reaction forces and moments as well as skin marker trajectories. Other advanced methods for inverse dynamics (i.e., residual elimination/reduction algorithms) typically alter the generalized accelerations of the model but may also include either some (Delp et al. 2007) or all of the BSIPs (Jackson et al. 2015) as design variables of the minimization process.

Most of the abovementioned methods for BSIPs assessment involve numerous skin markers, especially when all the segments of the human body (e.g., the 16 segments previously mentioned) are of interest. Therefore, another direction is to reduce the number of skin markers at its minimum while estimating the center of mass of the human body, typically for the analysis of the dynamic stability. Adapted segment definition, regression equations, and marker set have been dedicated for such specific applications (Tisserand et al. 2016; Yang and Pai 2014).

References

- Ackland TR, Blanksby BA, Bloomfield J (1988) Inertial characteristics of adolescent male body segments. *J Biomech* 21(4):319–327. doi:10.1016/0021-9290(88)90261-8
- Ayusawa K, Venture G, Nakamura Y (2014) Identifiability and identification of inertial parameters using the underactuated base-link dynamics for legged multibody systems. *Int J Robot Res* 33(3):446–468. doi:10.1177/0278364913495932
- Bauer JJ, Pavol MJ, Snow CM, Hayes WC (2007) MRI-derived body segment parameters of children differ from age-based estimates derived using photogrammetry. *J Biomech* 40(13):2904–2910. doi:10.1016/j.jbiomech.2007.03.006
- Bonnet V, Dumas R, Cappozzo A, Joukov V, Daune G, Kulić D, Fraise P, Andary S, Venture G (2017) A constrained extended Kalman filter for the optimal estimate of kinematics and kinetics of a sagittal symmetric exercise. *J Biomech*. doi:10.1016/j.jbiomech.2016.12.027
- Chandler RF, Clauser CE, McConville JT, Reynolds HM, Young JW (1975) Investigation of inertial properties of the human body. Aerospace Medical Research Laboratory, Wright-Patterson Air Force Base, Dayton
- Cheng C-K, Chen H-H, Chen C-S, Lee C-L, Chen C-Y (2000) Segment inertial properties of Chinese adults determined from magnetic resonance imaging. *Clin Biomech* 15(8):559–566. doi:10.1016/S0268-0033(00)00016-4
- Clauser CE, McConville JT, Young JW (1969) Weight, volume, and center of mass of segments of the human body. Aerospace Medical Research Laboratory, Wright-Patterson Air Force Base, Dayton
- Dao TT, Marin F, Pouletaut P, Charleux F, Aufaure P, Ho Ba Tho MC (2012) Estimation of accuracy of patient-specific musculoskeletal modelling: case study on a post polio residual paralysis subject. *Comput Methods Biomech Biomed Eng* 15(7):745–751. doi:10.1080/10255842.2011.558086
- Davidson PL, Wilson SJ, Wilson BD, Chalmers DJ (2008) Estimating subject-specific body segment parameters using a 3-dimensional modeller program. *J Biomech* 41(16):3506–3510. doi:10.1016/j.jbiomech.2008.09.021
- Davis RB III, Öunpuu S, Tyburski D, Gage JR (1991) A gait analysis data collection and reduction technique. *Hum Mov Sci* 10(5):575–587. doi:10.1016/0167-9457(91)90046-Z
- de Leva P (1996a) Adjustments to Zatsiorsky-Seluyanov's segment inertia parameters. *J Biomech* 29(9):1223–1230. doi:10.1016/0021-9290(95)00178-6
- de Leva P (1996b) Joint center longitudinal positions computed from a selected subset of Chandler's data. *J Biomech* 29(9):1231–1233. doi:10.1016/0021-9290(96)00021-8
- Delp SL, Anderson FC, Arnold AS, Loan P, Habib A, John CT, Guendelman E, Thelen DG (2007) OpenSim: Open-source software to create and analyze dynamic simulations of movement. *IEEE Trans Biomed Eng* 54(11):1940–1950. doi:10.1109/TBME.2007.901024
- Dempster WT (1955) Space requirements for the seated operator. Wright Air Development Center, Wright-Patterson Air Force Base, Dayton
- Drillis R, Contini R, Bluestein M (1964) Body segment parameters: a survey of measurement techniques. *Artif Limbs* 8(1):44–66
- Dumas R, Aissaoui R, Mitton D, Skalli W, de Guise JA (2005) Personalized body segment parameters from biplanar low-dose radiography. *IEEE Trans Biomed Eng* 52(10):1756–1763. doi:10.1109/TBME.2005.855711
- Dumas R, Cheze L, Verriest JP (2007a) Adjustments to McConville et al. and Young et al. body segment inertial parameters. *J Biomech* 40(3):543–553. doi:10.1016/j.jbiomech.2006.02.013
- Dumas R, Cheze L, Verriest JP (2007b) Corrigendum to “Adjustments to McConville et al. and Young et al. body segment inertial parameters”. *J Biomech* 40(7):1651–1652. doi:10.1016/j.jbiomech.2006.07.016
- Dumas R, Robert T, Cheze L, Verriest J-P (2015) Thorax and abdomen body segment inertial parameters adjusted from McConville et al. and Young et al. *Int Biomech* 2(1):113–118. doi:10.1080/23335432.2015.1112244

- Durkin JL, Dowling JJ, Andrews DM (2002) The measurement of body segment inertial parameters using dual energy X-ray absorptiometry. *J Biomech* 35(12):1575–1580. doi:10.1016/S0021-9290(02)00227-0
- Gainley KJ, Powers CM (2004) Determination of lower extremity anthropometric parameters using dual energy X-ray absorptiometry: the influence on net joint moments during gait. *Clin Biomech* 19(1):50–56. doi:10.1016/j.clinbiomech.2003.08.002
- Hinrichs RN (1990) Adjustments to the segment center of mass proportions of Clauser et al. (1969). *J Biomech* 23(9):949–951. doi:10.1016/0021-9290(90)90361-6
- Ho Hoang K-L, Mombaur K (2015) Adjustments to de Leva-anthropometric regression data for the changes in body proportions in elderly humans. *J Biomech* 48(13):3732–3736. doi:10.1016/j.jbiomech.2015.08.018
- Jackson JN, Hass CJ, Fregly BJ (2015) Residual elimination algorithm enhancements to improve foot motion tracking during forward dynamic simulations of Gait. *J Biomech Eng* 137(11):111002. doi:10.1115/1.4031418
- Jensen RK (1978) Estimation of the biomechanical properties of three body types using a photogrammetric method. *J Biomech* 11(8-9):349–358. doi:10.1016/0021-9290(78)90069-6
- Jovic J, Escande A, Ayusawa K, Yoshida E, Kheddar A, Venture G (2016) Humanoid and human inertia parameter identification using hierarchical optimization. *IEEE Trans Robot* 32(3):726–735. doi: 10.1109/TRO.2016.2558190
- Kadaba MP, Ramakrishnan HK, Wootten ME (1990) Measurement of lower extremity kinematics during level walking. *J Orthop Res* 8(3):383–392. doi:10.1002/jor.1100080310
- McConville JT, Churchill TD, Kaleps I, Clauser CE, Cuzzi J (1980) Anthropometric relationships of body and body segment moments of inertia. Aerospace Medical Research Laboratory, Wright-Patterson Air Force Base, Dayton
- Mungiole M, Martin PE (1990) Estimating segment inertial properties: comparison of magnetic resonance imaging with existing methods. *J Biomech* 23(10):1039–1046. doi:10.1016/0021-9290(90)90319-X
- Pearsall DJ, Reid G (1994) The study of human body segment parameters in biomechanics. *Sports Med* 18(2):126–140. doi:10.2165/00007256-199418020-00005
- Pearsall DJ, Reid JG, Livingston LA (1996) Segmental inertial parameters of the human trunk as determined from computed tomography. *Ann Biomed Eng* 24(2):198–210. doi:10.1007/BF02667349
- Pillet H, Bonnet X, Lavaste F, Skalli W (2010) Evaluation of force plate-less estimation of the trajectory of the centre of pressure during gait. Comparison of two anthropometric models. *Gait Posture* 31(2):147–152. doi:10.1016/j.gaitpost.2009.09.014
- Plagenhoef S (1971) Patterns of human motion: a cinematographic analysis. Prentice-Hall, Englewood Cliffs
- Reid JG, Jensen RK (1990) Human body segment inertia parameters: a survey and status report. *Exerc Sport Sci Rev* 18(1)
- Sreenivasa M, Chamorro CJG, Gonzalez-Alvarado D, Rettig O, Wolf SI (2016) Patient-specific bone geometry and segment inertia from MRI images for model-based analysis of pathological gait. *J Biomech* 49(9):1918–1925. doi:10.1016/j.jbiomech.2016.05.001
- Taddei F, Martelli S, Valente G, Leardini A, Benedetti MG, Manfrini M, Viceconti M (2012) Femoral loads during gait in a patient with massive skeletal reconstruction. *Clin Biomech* 27(3):273–280. doi:10.1016/j.clinbiomech.2011.09.006
- Tisserand R, Robert T, Dumas R, Chèze L (2016) A simplified marker set to define the center of mass for stability analysis in dynamic situations. *Gait Posture* 48:64–67. doi:10.1016/j.gaitpost.2016.04.032
- Valente G, Pitto L, Testi D, Seth A, Delp SL, Stagni R, Viceconti M, Taddei F (2014) Are subject-specific musculoskeletal models robust to the uncertainties in parameter identification? *PLoS One* 9(11):e112625. doi:10.1371/journal.pone.0112625
- Vaughan CL, Andrews JG, Hay JG (1982) Selection of body segment parameters by optimization methods. *J Biomech Eng* 104(1):38–44. doi:10.1115/1.3138301

- Verriest JP (2012) Automatic anthropometric personalization of a digital human model from a set of subject's photographs. *Work* 41(Suppl 1):4061–4068. doi:10.3233/WOR-2012-0071-4061
- Winter DA (2009) *Biomechanics and motor control of human movement*. Wiley, New York
- Wu G, Siegler S, Allard P, Kirtley C, Leardini A, Rosenbaum D, Whittle M, D'Lima DD, Cristofolini L, Witte H, Schmid O, Stokes I (2002) ISB recommendation on definitions of joint coordinate system of various joints for the reporting of human joint motion – part I: ankle, hip, and spine. *J Biomech* 35(4):543–548. doi:10.1016/S0021-9290(01)00222-6
- Wu G, van der Helm FCT, Veeger HEJ, Makhsous M, Van Roy P, Anglin C, Nagels J, Karduna AR, McQuade K, Wang X, Werner FW, Buchholz B (2005) ISB recommendation on definitions of joint coordinate systems of various joints for the reporting of human joint motion – part II: shoulder, elbow, wrist and hand. *J Biomech* 38(5):981–992. doi:10.1016/j.jbiomech.2004.05.042
- Yang F, Pai Y-C (2014) Can sacral marker approximate center of mass during gait and slip-fall recovery among community-dwelling older adults? *J Biomech* 47(16):3807–3812. doi:10.1016/j.jbiomech.2014.10.027
- Yeadon MR, Morlock M (1989) The appropriate use of regression equations for the estimation of segmental inertia parameters. *J Biomech* 22(6):683–689. doi:10.1016/0021-9290(89)90018-3
- Young JW, Chandler RF, Snow CC, Robinette KM, Zehner GF, Lofberg MS (1983) *Anthropometric and mass distribution characteristics of the adults female*. FAA Civil Aeromedical Institute, Oklahoma City
- Zatsiorsky VM, Seluyanov VN, Chugunova LG (1990) Methods of determining mass-inertial characteristics of human body segments. In: Chernyi GG, Regirer SA (eds) *Contemporary problems of biomechanics*. CRC Press, Massachusetts, pp 272–291